JOURNAL OF GUIDANCE, CONTROL, AND DYNAMICS
Vol. 32, No. 4, July–August 2009

Engineering Notes

ENGINEERING NOTES are short manuscripts describing new developments or important results of a preliminary nature. These Notes should not exceed 2500 words (where a figure or table counts as 200 words). Following informal review by the Editors, they may be published within a few months of the date of receipt. Style requirements are the same as for regular contributions (see inside back cover).

Hybrid Genetic Algorithm Collocation Method for Trajectory Optimization

Kamesh Subbarao* and Brandon M. Shippey†
University of Texas at Arlington, Arlington, Texas 76019-0018

DOI: 10.2514/1.41449

Introduction

RESEARCH of recent decades has uncovered many advances in the development of numerical trajectory optimization. These methods are attempts to solve discretized versions of some form of an optimal control problem that, in general, cannot be solved analytically using Pontryagin's minimum principle [1]. Numerous techniques exist, each one parameterizing the problem and enforcing the equations of motion differently. One such technique is that of differential inclusions, which constrains the discretized states at adjacent nodes to lie on the attainable sets given the admissible control inputs [2]. Alternatively, direct shooting methods discretize the control history and integrate the equations of motion to obtain the state histories and evaluate the constraint violations [3]. A third technique, collocation, enforces the equations of motion through constraints on the derivative of an interpolating function and the state equations [4]. These various methods have been applied to a number of problems, including space vehicle reentry trajectories [5], kinematic path planning for unmanned aerial and ground vehicles [6], spacecraft slewing maneuvers [7,8], and low-thrust orbit transfers [9–12].

Given this context, the present work seeks to implement a hybrid genetic algorithm collocation method for direct optimization of trajectories. The initial guesses for the state and control histories used in the collocation method are interpolated from the best candidate solution of a genetic algorithm. The control histories are not assumed to take a specific form, because for the general problem, no prior knowledge of the nature of the optimal solution is available at the outset. We use an off-the-shelf, freely available, implementation of a simple genetic algorithm without modification, and the collocation method is an implementation of the Hermite–Legendre–Gauss–Lobatto method (see [13]). The customized implementation requires the specification of certain user choices [control filtering in the genetic algorithm (GA) phase, number of intervals, and polynomial order], cost function, weighting coefficients for the cost function, and equality and inequality constraints.

Received 7 October 2008; revision received 24 March 2009; accepted for publication 24 March 2009.

*Assistant Professor, Box 19018, 211 Woolf Hall, West First Street, Department of Mechanical & Aerospace Engineering; subbarao@uta.edu. Lifetime Member AIAA.

†Graduate Student, Department of Mechanical & Aerospace Engineering; currently Engineer, Orbital Sciences Corporation, Chandler, AZ; brandon.shippey@mavs.uta.edu.

Problem Description

We seek to solve the following constrained optimal control problem. The cost function J to be minimized is the Bolza cost function including the Mayer term $\epsilon[\cdot]$ and the Lagrange term $L[\cdot]$:

$$J = \epsilon[\mathbf{x}(t_f), \mathbf{p}, t_f] + \int_{t_0}^{t_f} L[\mathbf{x}(t), \mathbf{u}(t), \mathbf{p}, t]\mathrm{d}t \tag{1}$$

The cost function and the terms in Eq. (1) follow the standard notation described in [14]. The cost is to be minimized subject to 1) state constraints, 2) control constraints, 3) endpoint constraints, 4) path constraints, and 5) upper and lower bounds on states, controls, and system parameters (box constraints). Under the general framework mentioned previously, we seek to find minimum-time low-thrust Earth–Mars transfer trajectories. The optimal control problem is solved using the Hermite–Legendre–Gauss–Lobatto (HLGL) collocation [13] technique that is initialized (state and control time histories) by a genetic algorithm.

Hermite–Legendre–Gauss–Lobatto Collocation

The specific details of this technique and other collocation techniques can be found in [11–13,15]. The optimal solution is obtained by minimizing the collocation error residuals over a set of time subintervals and explicitly incorporating the problem constraints. However, this requires that the designer provide an initial state and control history for the nonlinear programming (NLP). The collocation techniques are, in general, quite robust to initial guesses; however, in certain cases, this associated subproblem is most likely as complex as the original problem. In general, to provide a reasonable initial guess, we conduct a random search through the initial condition space that would result in a feasible initial trajectory. This crucial step is implemented via a genetic algorithm that is discussed next.

Initialization via Genetic Algorithm

As a primary tool to optimize a discrete approximation to a continuous optimal control problem, the genetic algorithm is not so attractive [3]. However, initialization of the NLP requires only that the candidate solution used for initialization be within the domain of convergence of the particular quasi-Newton algorithm. This means that the initialization need not meet all constraints or be optimal. The genetic algorithm can quickly locate candidate solutions of this quality. The simple genetic algorithm applied in this work is based upon the procedure outlined in [16]. The algorithm used here employs a simple random selection of parent pairs: crossover and mutation. Several of these functions are customizable via parameters or have algorithmic variations. For instance, though we use binary encoded chromosomes, real-valued chromosomes may be used. This type of chromosome has been used for initialization of an NLP solution in [17]. Note that a GA can provide approximate solutions that are close to optimal, yet infeasible. This is a potential drawback to the proposed hybrid approach, because the GA provides the initial condition to the NLP. However, this is also true of other approximate initialization schemes for a highly constrained problem.

Low-Thrust Interplanetary (Earth–Mars) Transfer

Problem Statement

Given the governing dynamic equations of motion described in this section, the solution to the transfer trajectory design problem should yield a minimum-time low-thrust transfer between Earth and Mars. The problem definition, geometries, and governing equations of motion are all adopted from [9] to provide a consistent benchmark for comparison. The formal statement indicates the following:

1) The spacecraft should begin in a geosynchronous orbit and end in an areosynchronous orbit (about Mars).

2) The transfer should occur in minimum time.

In the context of the optimal control problem described previously, the cost function to be minimized is given by

$$J = t_{f_1} + t_{f_2} + t_{f_3}$$

where t_{f_1}, t_{f_2}, and t_{f_3} are the time lengths of the geocentric, heliocentric, and areocentric trajectory segments, respectively. The nonlinear state dynamics describe the two-body motion of a point mass about the sun, Earth, or Mars. The simplification of the model to two dimensions throughout the trajectory relies upon the assumption that the orbits of Earth and Mars are coplanar. The equations of motion are

$$\dot{r} = v_r \qquad \dot{\theta} = (v_\theta/r) \qquad \dot{v}_r = (v_\theta^2/r) - (\mu/r^2) + a_T \sin\beta$$
$$\dot{v}_\theta = -(v_r v_\theta/r) + a_T \cos\beta \tag{2}$$

where r and θ are the polar coordinates of the spacecraft shown in Fig. 1a. The states v_r and v_θ are the radial and tangential components of the velocity vector. *The parameter a_T is the control acceleration magnitude, which is held constant at* $0.0001g$. The control input β is the thrust angle measured positive upward from the local horizon, as shown in Fig. 2. The gravitational parameter μ is normalized to 1 $\mathrm{DU}^3/\mathrm{TU}^2$ for all three segments. The units DU and TU are the normalized astronomical distance unit and time unit, respectively. They are defined differently for each segment and can be converted between segments easily. Note that the state names used in Eqs. (2) are appropriate for the geocentric segment of the trajectory only. Though the form of the dynamics is the same for each segment, description of the intersegment constraints requires that different state names be applied for each segment. The geocentric states r, θ, v_r, and v_θ are replaced by R, η, v_R, and v_η during heliocentric flight and ρ, δ, v_ρ, and v_δ during areocentric flight. Because each segment of the trajectory has its own endpoint, path, and box constraints, they are treated separately. Constraints involving more than one segment are discussed later in this section.

The first segment consists of a geocentric trajectory (the spacecraft is influenced only by the gravity of Earth) beginning from a circular geosynchronous orbit to a given final radius. The endpoint constraints include the initial and final radii and the initial radial and tangential velocities. The initial radius is calculated as that of a circular orbit with a period of $P = 1$ day:

$$r = \left(\frac{\mu}{(2\pi/P)^2}\right)^{1/3} = 6.6107R_E \tag{3}$$

The final radius is chosen to be the radius of the sphere of influence for Earth, $145R_E$, in keeping with the example in [9] for comparison. The initial radial velocity is zero for a circular orbit, and the initial tangential velocity is calculated by

$$v_\theta = \sqrt{\frac{\mu}{r}} = 0.38893R_E/\mathrm{TU}_E \tag{4}$$

for circular orbits [18].

The third (areosynchronous) segment requires similar constraints to those in the geosynchronous segment. The endpoint constraints include initial radius, final radius, final radial velocity, and final tangential velocity. The initial radius is the radius of the sphere of influence for Mars, $170R_M$, in keeping with the example in [9]. The final radius of $\rho = 6.0236R_M$ is calculated by Eq. (3) using areocentric coordinates and a period equal to the rotational period of Mars, 1.0260 days [18]. The final radial velocity is zero for a circular orbit, and the final tangential velocity of $v_\delta = 0.40745R_M/\mathrm{TU}_M$ is calculated by Eq. (4) using the areocentric orbit radius found previously.

Between the geocentric and heliocentric segments, the states are related by the constraints of Eqs. (5), and between the heliocentric and areocentric segments, they are related by those of Eqs. (6):

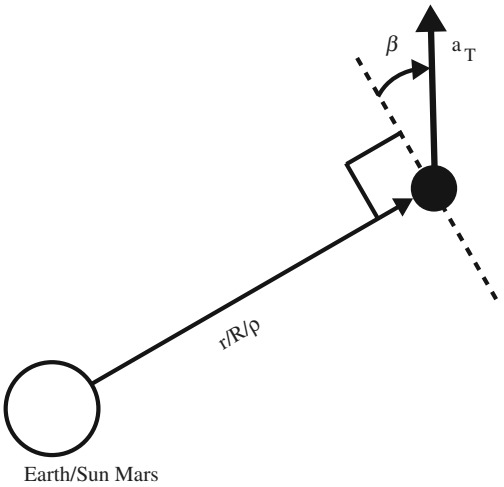

Fig. 2 Control of the spacecraft (thrust angle).

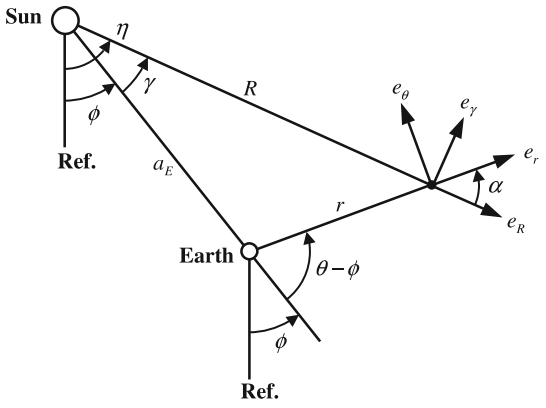

a) Heliocentric/geocentric coordinate transformation

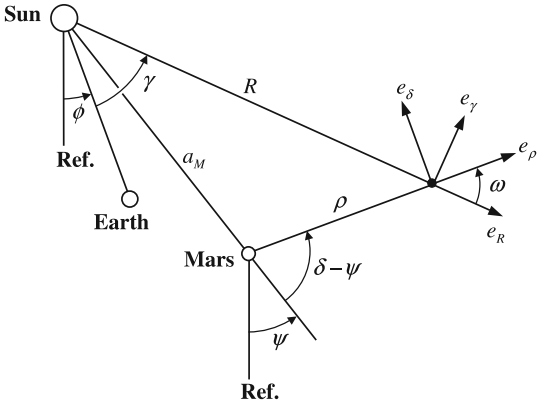

b) Heliocentric/areomcentric coordinate transformation

Fig. 1 Geometry for transformations between heliocentric and planetocentric coordinates.

$$R\cos\alpha - r - a_E\cos(\theta-\phi) = 0 \quad R\sin\alpha - a_E\sin(\theta-\phi) = 0$$
$$v_\eta\cos\alpha(1+\tan^2\alpha) - a_E\dot{\phi}\cos(\theta-\phi) - v_\theta$$
$$- a_E\dot{\phi}\sin(\theta-\phi)\tan\alpha - v_r\tan\alpha = 0$$
$$v_R\cos\alpha - a_E\dot{\phi}\sin(\theta-\phi) - v_r + v_\eta\sin\alpha = 0 \tag{5}$$

$$R\sin\omega - a_M\sin(\delta-\psi) = 0$$
$$R\cos\omega - a_M\cos(\delta-\psi) - \rho = 0$$
$$v_\eta\cos\omega - v_R\sin\omega - a_M\dot{\psi}\cos(\delta-\psi) - v_\delta = 0$$
$$v_R\cos\omega + v_\eta\sin\omega - a_M\dot{\psi}\sin(\delta-\psi) - v_\rho = 0 \tag{6}$$

In the preceding expressions, $\alpha = \theta - \eta$ and $\omega = \delta - \eta$. The orbit angles of Earth and Mars at the points of transition between segments are

$$\phi = \dot{\phi}t_{f_1} \tag{7}$$

for Earth at time t_{f_1} and

$$\psi = \text{MLA} + \dot{\psi}(t_{f_1} + t_{f_2}) \tag{8}$$

for Mars at time $t_{f_1} + t_{f_2}$. In Eqs. (7) and (8), the mean motions of the planetary orbits are

$$\dot{\phi} = \sqrt{\frac{\mu}{a_E^2}} = 1 \text{ rad/TU}_S \tag{9}$$

$$\dot{\psi} = \sqrt{\frac{\mu}{a_M^2}} = 0.53169 \text{ rad/TU}_S \tag{10}$$

where $a_E = 1$ AU and $a_M = 1.5237$ AU are the circular orbital radii of Earth and Mars about the sun, respectively [18]. The parameter MLA is the angle by which Mars leads Earth at the beginning of the geocentric segment. The specific choice of MLA = 0.9666 rad conforms to the example in [9].

GA Considerations

Special considerations must be addressed regarding the setup of this problem in the framework of the GA search. This problem presents some additional complications due to the multiple segments of the trajectory, each having its own set of dynamics and boundary conditions. Examination of the equations of motion reveals that when the spacecraft comes close to the attracting body, the natural frequency of the system is increased. To sufficiently capture the behavior of the spacecraft, this requires a high density of nodes in both the GA and HLGL discretizations. However, the high density of nodes adversely affects the evolution and convergence of the GA, because the control value of each node has less effect on the trajectory overall. One possible way to address this issue is to filter the control input signal, making trends in the control history more prevalent and smoothing the actual thrust-angle history. This is apparent in Figs. 3–5.

The filter is applied in each segment of the trajectory. The thrust angle is appended to the state vector. Its time derivative is

$$\dot{\beta} = -\lambda(\beta - \beta_c) \tag{11}$$

where β_c is the commanded thrust angle (control variable). The gain λ is 10^{-2} for the geocentric segment, 1 for the heliocentric segment, and 5×10^{-4} for the areocentric segment. Equation (11) is appended to the equations of motion in the GA phase, increasing the state-space order by one. For this case, β_c is now treated as the control variable. It is possible to constrain the control rates this way, if needed.

The geocentric segment has three known initial conditions (ICs) [namely, $r(0)$, $v_r(0)$, and $v_\theta(0)$] and only one known final condition (FC) [i.e., $r(t_{f_1})$]. Because it is better to ensure that the three ICs are met while letting the GA search only for the FC, the geocentric phase is integrated forward, initialized by the IC. The initial orbit angle $\theta(0)$ is included as an optimization parameter in the GA search. In contrast, three of the FCs of the areocentric segment are known [$\rho(t_{f_3})$, $v_\rho(t_{f_3})$, and $v_\delta(t_{f_3})$], whereas only one IC is known [$\rho(0)$]. In this case, the GA will be more effective if only the initial radius is searched for. Therefore, the choice is to integrate the areocentric segment backward.

For the heliocentric segment, none of the boundary conditions are known. The marching integration must be initialized by transforming the coordinates at the boundary of an adjacent segment. The coordinate transformation at the other boundary may be enforced through constraint violation penalties in the GA cost function. The choice is to integrate the heliocentric segment forward, initializing the states by transforming the final geocentric states (r, θ, v_r, and v_θ) into heliocentric coordinates (R, η, v_R, and v_η). The transformation is given by

$$R = \sqrt{(r + a_E\cos(\theta-\phi))^2 + (a_E\sin(\theta-\phi))^2}$$
$$\alpha = \sin^{-1}\left(\frac{a_E}{R}\sin(\theta-\phi)\right)$$
$$\eta = \theta - \alpha$$
$$v_\eta = \frac{a_E\dot{\phi}\cos(\theta-\phi) + v_\theta + a_E\dot{\phi}\sin(\theta-\phi)\tan\alpha + v_r\tan\alpha}{\cos\alpha(1+\tan^2\alpha)}$$
$$v_R = \frac{a_E\dot{\phi}\sin(\theta-\phi) + v_r - v_\eta\sin\alpha}{\cos\alpha} \tag{12}$$

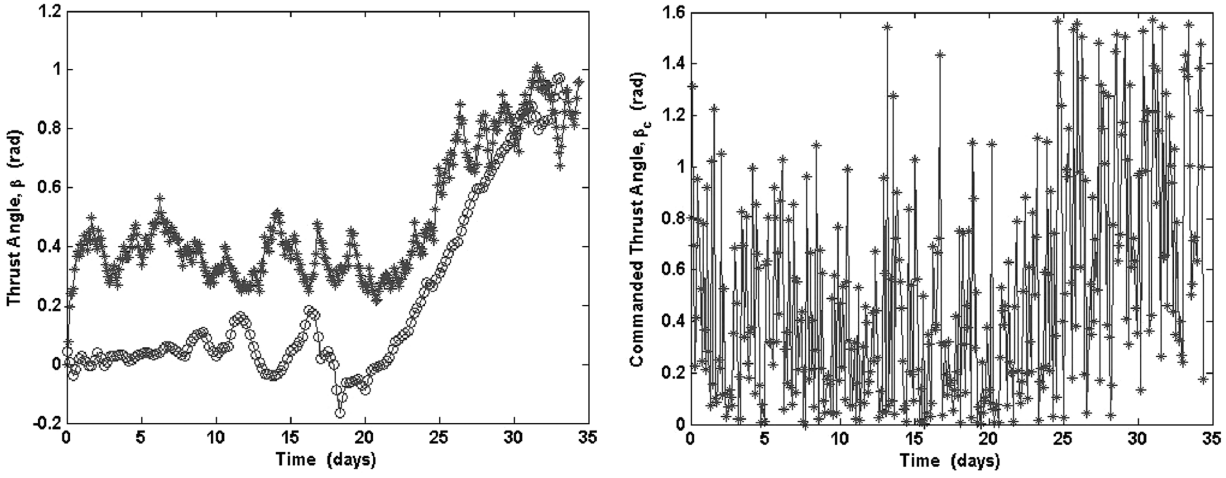

a) Thrust angle ('-*' GA, '-o' HLGL) b) Commanded thrust angle (GA only)

Fig. 3 Results for the geocentric segment commanded and actual thrust angle.

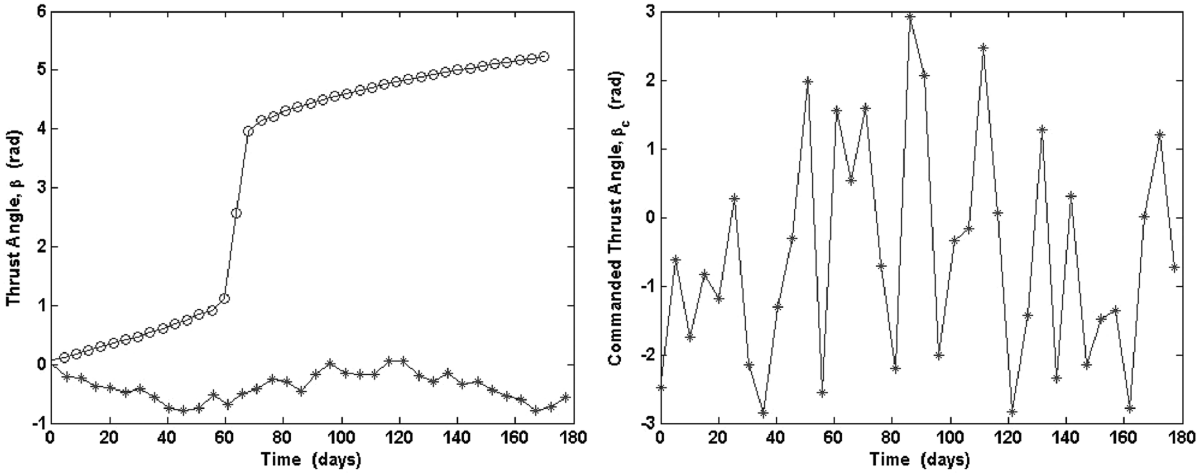

a) Thrust angle ('-*' GA, '-o' HLGL) **b) Commanded thrust angle (GA only)**

Fig. 4 Results for the heliocentric segment commanded and actual thrust angle.

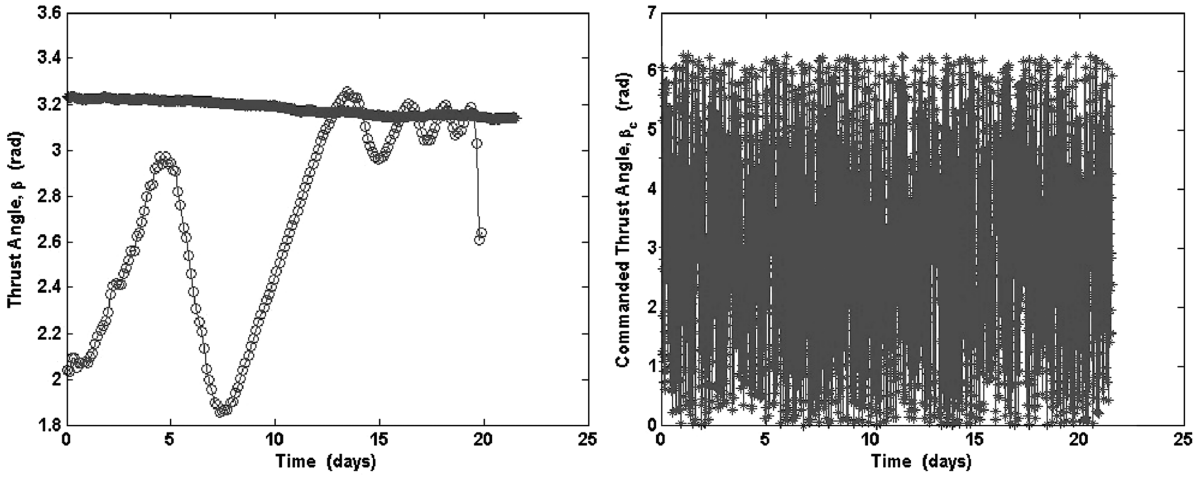

a) Thrust angle ('-*' GA, '-o' HLGL) **b) Commanded thrust angle (GA only)**

Fig. 5 Results for the areocentric segment commanded and actual thrust angle.

evaluated at time t_{f_1}. The penalties enforcing the constraints between the heliocentric FCs and the areocentric ICs are derived from Eqs. (6) and are provided later in this section.

The cost function used for ranking includes the cost function of the minimum-time problem definition plus penalties for any constraint violations that apply:

$$J = J_{\text{seg1}} + J_{\text{seg2}} + J_{\text{seg3}} + J_{2/3} \tag{13}$$

where the components J_{seg} correspond to penalties applying to the segment indicated by the subscript, and $J_{2/3}$ is the penalty for violation of the constraints that enforce the transformation of coordinates at the boundary between the heliocentric and areocentric segments. For the geocentric segment, the penalties include the final time, final orbit radius error, and the following constraint violations evaluated for all nodes: maximum orbit radius, minimum orbit radius, and maximum tangential velocity. The penalties are expressed as

$$J_{\text{seg1}} = t_{f_1} + 10^4 |r_{N_1} - 145R_E| + \sum_{i=1}^{N_1} w_{ru} |r_i - 145R_E| + \sum_{i=1}^{N_1} w_{rl} |r_i - 6.6107R_E| + \sum_{i=1}^{N_1} w_{v\theta} |v_{\theta,i} - 0.38893R_E/\text{TU}_E| \tag{14}$$

where N_1 is the number of discrete nodes in the Runge–Kutta integration in the geocentric segment, and the weights are

$$w_{ru} = \begin{cases} 1, & r_i > 145R_E \\ 0, & r_i \le 145R_E \end{cases} \tag{15}$$

$$w_{rl} = \begin{cases} 1, & r_i < 6.6107R_E \\ 0, & r_i \ge 6.6107R_E \end{cases} \tag{16}$$

$$w_{v\theta} = \begin{cases} 1, & v_\theta > 0.38893R_E/\text{TU}_E \\ 0, & v_\theta \le 0.38893R_E/\text{TU}_E \end{cases} \tag{17}$$

For the heliocentric segment, the penalties include the final time t_{f_2} and penalties evaluated at all nodes for violation of maximum and minimum orbit radii. The penalties are

$$J_{\text{seg2}} = 10^{-2} t_{f_2} + \sum_{i=1}^{N_2} w_{Ru} |R_i - 1.62 \text{ AU}| + \sum_{i=1}^{N_2} w_{Rl} |R_i - 0.9 \text{ AU}| \tag{18}$$

where N_2 is the number of discrete nodes used in the Runge–Kutta integration for the heliocentric segment, and the weights are

$$w_{Ru} = \begin{cases} 1, & R_i > 1.62 \text{ AU} \\ 0, & R_i \le 1.62 \text{ AU} \end{cases} \tag{19}$$

$$w_{Rl} = \begin{cases} 1, & R_i < 0.9 \text{ AU} \\ 0, & R_i \ge 0.9 \text{ AU} \end{cases} \tag{20}$$

For the areocentric segment, the penalties include the final time t_{f_3}, the error of the initial radius, and the following constraint violations evaluated at all nodes: maximum radial velocity, maximum tangential velocity, and maximum and minimum orbit radius. The penalties are expressed as

$$J_{\text{seg3}} = t_{f_3} + 10^2|\rho_{N_3} - 170R_M| + \sum_{i=1}^{N_3} w_{\rho u}|\rho_i - 170R_M| + \sum_{i=1}^{N_3} w_{v\rho}|v_{\rho,i}| + \sum_{i=1}^{N_3} w_{\rho l}|\rho_i - 6.0236R_M| + \sum_{i=1}^{N_3} w_{v\delta}|v_{\delta,i} - 0.40745R_M/\text{TU}_M| \tag{21}$$

where N_3 is the number of discrete nodes in the Runge–Kutta integration for the areocentric segment, and the weights are

$$w_{\rho u} = \begin{cases} 1, & \rho_i > 170R_M \\ 0, & \rho_i \le 170R_M \end{cases} \tag{22}$$

$$w_{\rho l} = \begin{cases} 1, & \rho_i < 6.0236R_M \\ 0, & \rho_i \ge 6.0236R_M \end{cases} \tag{23}$$

$$w_{v\rho} = \begin{cases} 1, & v_{\rho,i} > 0R_M/\text{TU}_M \\ 0, & v_{\rho,i} \le 0R_M/\text{TU}_M \end{cases} \tag{24}$$

$$w_{v\delta} = \begin{cases} 1, & v_{\delta,i} > 0.40745R_M/\text{TU}_M \\ 0, & v_{\delta,i} \le 0.40745R_M/\text{TU}_M \end{cases} \tag{25}$$

Finally, the component of the cost penalizing constraint violations at the boundary connecting the heliocentric and areocentric segments is formulated from the constraints of Eqs. (6) and is expressed as

$$J_{2/3} = |c_1| + |c_2| + |c_3| + |c_4| \tag{26}$$

where

$$c_1 = R\sin\omega - a_M\sin(\delta - \psi) \tag{27}$$

$$c_2 = R\cos\omega - a_M\cos(\delta - \psi) - \rho \tag{28}$$

$$c_3 = v_\eta\cos\omega - v_R\sin\omega - a_M\dot{\psi}\cos(\delta - \psi) - v_\delta \tag{29}$$

$$c_4 = v_R\cos\omega + v_\eta\sin\omega - a_M\dot{\psi}\sin(\delta - \psi) - v_\rho \tag{30}$$

Results

For the genetic algorithm, the chromosome uses real encoding for the parameters rather than binary encoding. The genetic algorithm is parameterized as follows. The population is held at 150 chromosomes and is propagated for 75 generations. The final times of the three trajectory segments, as well as the initial orbit angle of the geocentric segment and the final orbit angle of the areocentric

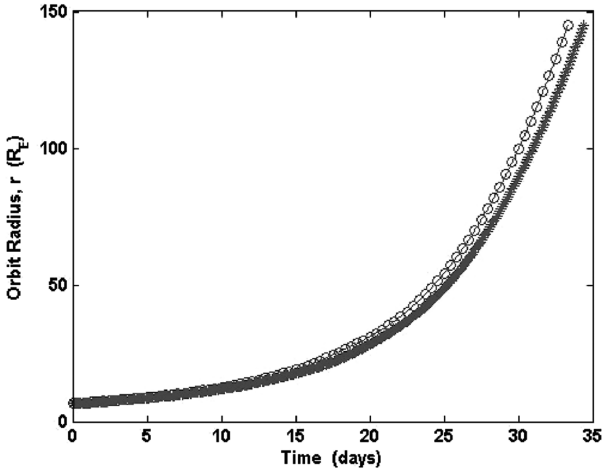

a) Orbit radius ('-*' GA, '-o' HLGL)

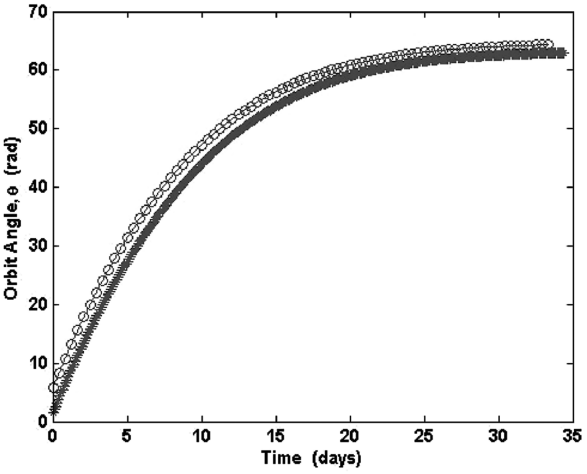

b) Orbit angle ('-*' GA, '-o' HLGL)

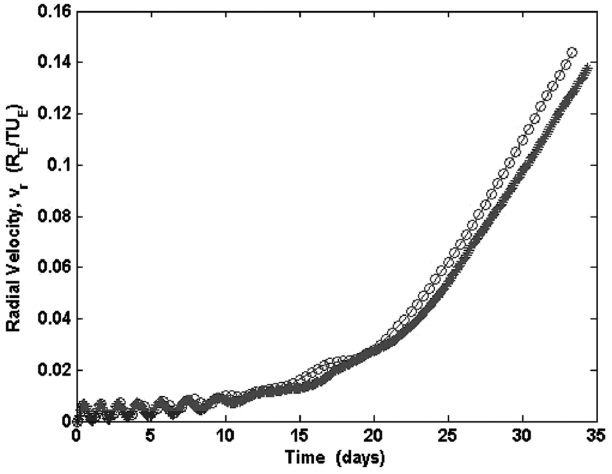

c) Radial velocity ('-*' GA, '-o' HLGL)

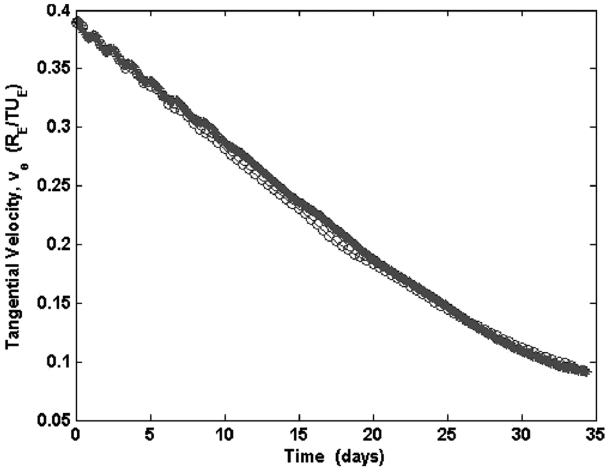

d) Tangential velocity ('-*' GA, '-o' HLGL)

Fig. 6 Results for the heliocentric segment states.

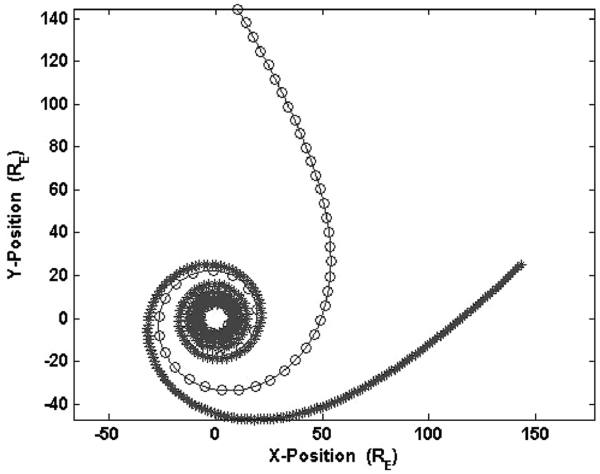

Fig. 7 Earth departure spiral (* GA and ∘ HLGL).

segment, are treated as optimization parameters in the chromosomes. The lower and upper bounds on the initial orbit angle θ for the geocentric segment and the final orbit angle δ for the areocentric segment are 0 and 2π rad, respectively. The HLGL collocation phase of the optimization is parameterized such that the nodes and intervals are the same is are used in [9]. All three segments use the third-order Hermite interpolating polynomial, making the collocation equivalent to the Hermite–Simpson method. The geocentric and areocentric segments have 80 time intervals each, whereas the heliocentric segment has 20 intervals. The convergence criteria for the NLP are a maximum constraint violation of 1×10^{-12} (`TolCon`) and a reduction in the cost function of less than 2×10^{-6} (`TolFun`) for one iteration. The complete framework is implemented in MATLAB® (R2007b) on a personal computer (Intel Pentium IV) with 512 MB RAM running at 2.4 GHz processor speed.

The final resulting candidate solution by the genetic algorithm is shown in Figs. 6–11. A few of the problem requirements are met very well. For instance, the final orbit radius of the geocentric segment (resulting in $145.000R_E$) and the initial orbit radius of the areocentric segment ($170.004R_M$) are satisfied very well. It is also apparent from Fig. 3a that the thrust angle follows the upward trend shown later in the HLGL solution, as well as in [9].

The poorly met requirements are most noticeable in the final conditions of the heliocentric trajectory. In this segment, the spacecraft overshoots the sphere of influence of Mars by a significant distance, even though error penalties are applied at the boundary between the heliocentric and areocentric segments to ensure proper continuity of position and velocity. This is also revealed in Fig. 8c. The more accurate solution by the HLGL collocation phase shows that the radial velocity of the spacecraft should decrease near the end of the heliocentric segment as its position approaches Mars.

Neither the thrust angle in the heliocentric nor areocentric segments follow the trends given by the HLGL solution. The results given by the genetic algorithm may be improved through some adjustment of parameters in the cost function and the population. The final GA solution may also be improved by propagating the population for more generations, allowing better candidate solutions

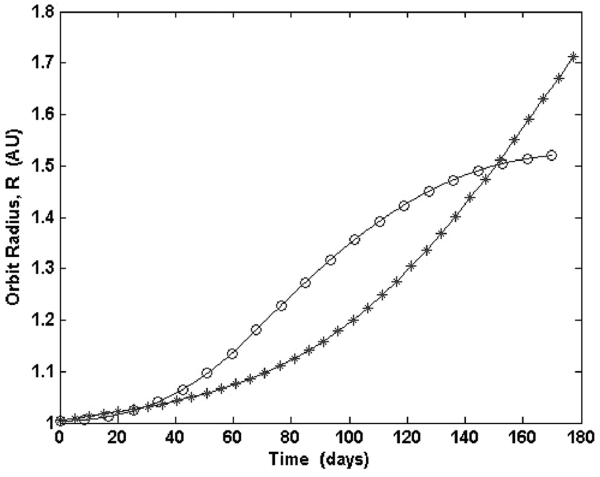

a) Orbit radius ('-*' GA, '-o' HLGL)

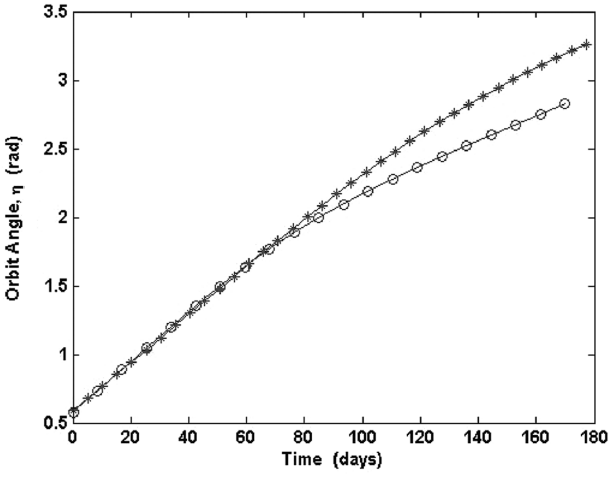

b) Orbit angle ('-*' GA, '-o' HLGL)

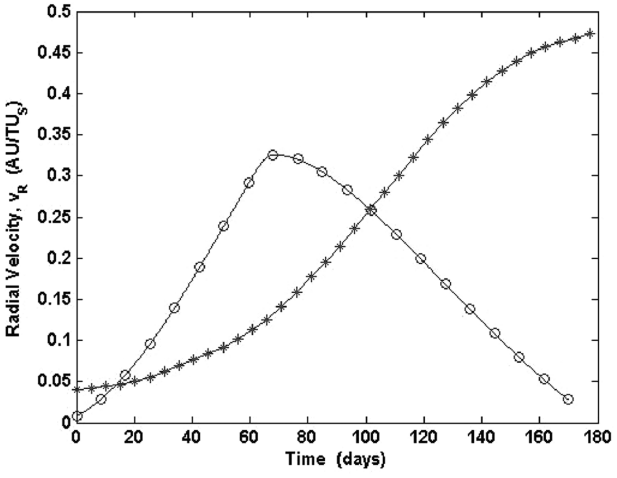

c) Radial velocity ('-*' GA, '-o' HLGL)

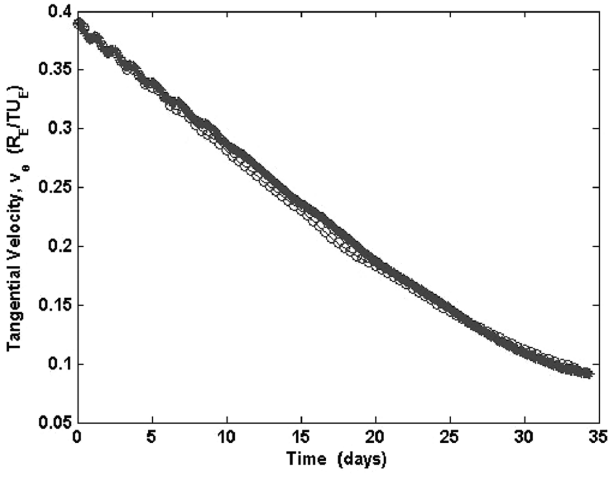

d) Tangential velocity ('-*' GA, '-o' HLGL)

Fig. 8 Results for the geocentric segment states.

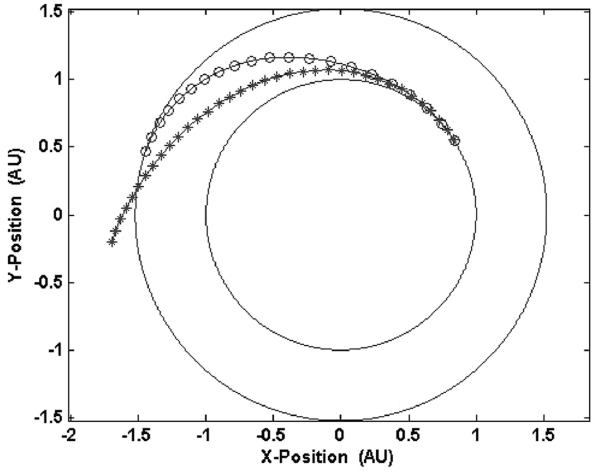

Fig. 9 Heliocentric transfer orbit (* GA and ∘ HLGL).

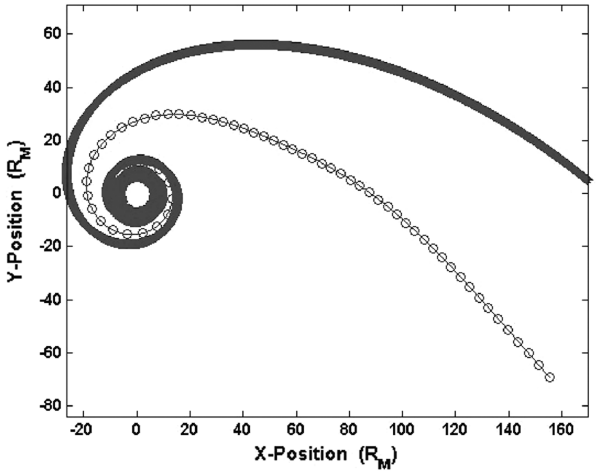

Fig. 11 Mars capture spiral (* GA and ∘ HLGL).

to evolve. Although many improvements to the GA solution may be possible, the inaccurate result is shown to provide a reasonable initialization for the HLGL collocation phase.

Upon examination of the final result of the HLGL collocation phase, all of the problem boundary-condition constraints are very well met, including the constraints relating the states of the heliocentric segment to the planetocentric segments at their boundaries. The final times of the three segments are given in Table 1, along with the final times published in the literature [9]. We see a good agreement, in general, between the published results and the results provided in this study.

As the iterations of the collocation phase of the optimization progressed, the convergence criteria were adjusted to be more strict. Using the new convergence criteria, the NLP was reinitialized and allowed to converge again. This was repeated a few (2 or 3) times to improve the results. In the literature we have seen, optimization problems such as these have typically used customized codes as in [9] or other specialized optimizers such as SNOPT [19]. Our work

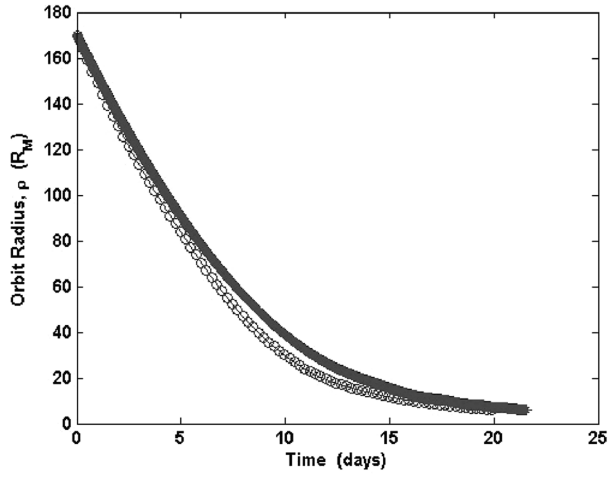

a) Orbit radius ('-*' GA, '-o' HLGL)

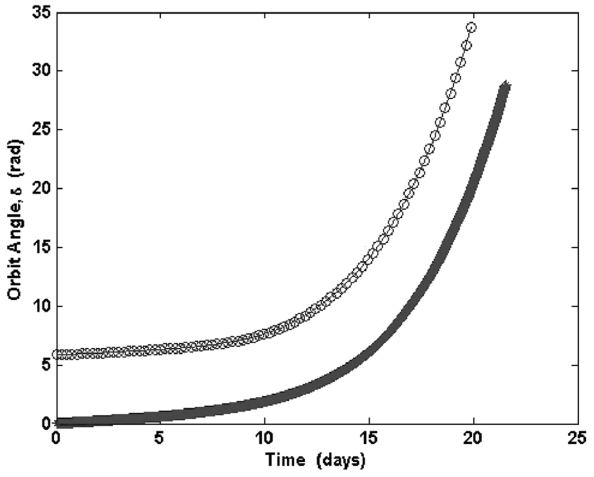

b) Orbit angle (`-*' GA, `-o' HLGL)

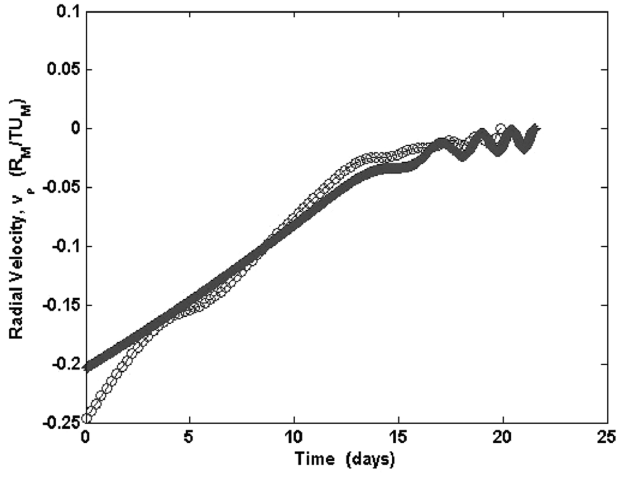

c) Radial velocity ('-*' GA, '-o' HLGL)

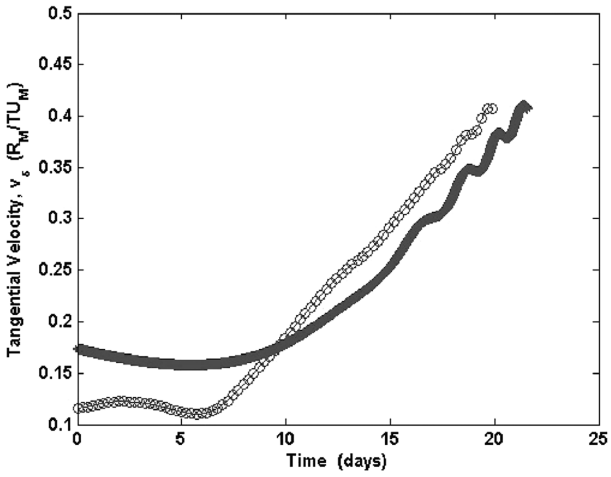

d) Tangential velocity ('-*' GA, 'o' HLGL)

Fig. 10 Results for the areocentric segment states.

Table 1 Final times for the geocentric, heliocentric, and areocentric segments

	Final time, days	
Segment	HLGL	[9]
1 (geocentric)	33.88	33.08
2 (heliocentric)	169.06	169.78
3 (areocentric)	20.05	19.28

presented here was implemented within the MATLAB environment using `fmincom`, a constrained optimization routine available with the Optimization Toolbox. It is quite possible that the results can be further improved by using a different custom optimization routine.

Conclusions

In this Note, we presented a hybrid numerical optimization technique for synthesis of trajectories using a direct Hermite–Legendre–Gauss–Lobatto collocation technique. The minimum-time low-thrust transfer trajectory from a geocentric circular orbit to an areocentric circular orbit was computed. The initial guesses for the nonlinear programming problem were obtained by searching through the state space for feasible candidate solutions via a genetic algorithm with a shooting method. The results obtained compare very favorably with published results.

References

[1] Bryson, A. E., and Ho, Y. C., *Applied Optimal Control*, Blaisdell, London, 1969, pp. 108–109.

[2] Seywald, H., "Trajectory Optimization Based on Dierential Inclusion," *Journal of Guidance, Control, and Dynamics*, Vol. 17, No. 3, 1994, pp. 480–487. doi:10.2514/3.21224

[3] Betts, J. T., "Survey of Numerical Methods for Trajectory Optimization," *Journal of Guidance, Control, and Dynamics*, Vol. 21, No. 2, Mar.–Apr. 1998, pp. 193–207. doi:10.2514/2.4231

[4] Hargraves, C. R., and Paris, S. W., "Direct Trajectory Optimization Using Nonlinear Programming and Collocation," *Journal of Guidance, Control, and Dynamics*, Vol. 10, No. 4, 1987, p. 338. doi:10.2514/3.20223

[5] Bonnans, J. F., and Launay, G., "Large-Scale Direct Optimal Control Applied to a Re-Entry Problem," *Journal of Guidance, Control, and Dynamics*, Vol. 21, No. 6, Nov.–Dec. 1998, pp. 996–1000. doi:10.2514/2.4337

[6] Bollino, K. P., Lewis, L. R., Sekhavat, P., and Ross, I. M., "Pseudospectral Optimal Control: A Clear Road for Autonomous Intelligent Path Planning," AIAA Infotech@Aerospace Conference and Exhibit, AIAA Paper 2007-2831, Rohnert Park, CA, May 2007.

[7] Seywald, H., Kumar, R. R., and Deshpande, S. M., "Genetic Algorithm Approach for Optimal Control Problems with Linearly Appearing Controls," *Journal of Guidance, Control, and Dynamics*, Vol. 18, No. 1, Jan.–Feb. 1995, pp. 177–182. doi:10.2514/3.56673

[8] Proulx, R. J., and Ross, I. M., "Time-Optimal Reorientation of Asymmetric Rigid Bodies," AIAA/AAS Astrodynamics Specialist Conference, American Astronautical Society Paper 01-384, July–Aug. 2001, pp. 1207–1227.

[9] Tang, S., and Conway, B. A., "Optimization of Low-Thrust Interplanetary Trajectories Using Collocation and Nonlinear Programming," *Journal of Guidance, Control, and Dynamics*, Vol. 18, No. 3, May–June 1995, pp. 599–604. doi:10.2514/3.21429

[10] Herman, A. L., and Spencer, D. B., "Optimal, Low-Thrust Earth-Orbit Transfers Using Higher-Order Collocation Methods," *Journal of Guidance, Control, and Dynamics*, Vol. 25, No. 1, Jan.–Feb. 2002, pp. 40–47. doi:10.2514/2.4873

[11] Hermann, H. L., and Conway, B. A., "Direct Optimization using Collocation Based on High-Order Gauss-Lobatto Quadrature Rules," *Journal of Guidance, Control, and Dynamics*, Vol. 19, No. 3, 1996, pp. 592–599. doi:10.2514/3.21662

[12] Enright, P. J., and Conway, B. A., "Discrete Approximations to Optimal Trajectories Using Direct Transcription and Nonlinear Programming," *Journal of Guidance, Control, and Dynamics*, Vol. 15, No. 4, 1992, pp. 994–1002. doi:10.2514/3.20934

[13] Williams, P., "Hermite–Legendre–Gauss–Lobatto Direct Transcription Methods in Trajectory Optimization," *AAS/AIAA Space Flight Mechanics Conference*, American Astronautical Society Paper 05-131, Copper Mountain, CO, Jan 23–27 2005.

[14] Bryson, A. E., and Ho, Y. C., *Applied Optimal Control*, Blaisdell, London, 1969, Chap. 6.

[15] Paris, S. W., Riehl, J. P., and Sjauw, W. K., "Enhanced Procedures for Direct Trajectory Optimization Using Nonlinear Programming and Implicit Integration," AIAA/AAS Astrodynamics Specialist Conference, AIAA Paper 2006-6309, Keystone, CO, 2006.

[16] Chippereld, A., Flemming, P., Pohlheim, H., and Fonseca, C., "Genetic Algorithm Toolbox User's Guide," Department of Automatic Control and Systems Engineering, Univ. of Sheffield, Sheffield, England, U.K., 1994.

[17] Yokoyama, N., and Suzuki, S., "Modied Genetic Algorithm for Constrained Trajectory Optimization," *Journal of Guidance, Control, and Dynamics*, Vol. 28, No. 1, Jan.–Feb. 2005, pp. 139–144. doi:10.2514/1.3042

[18] Vallado, D. A., *Fundamentals of Astrodynamics and Applications*, 2nd ed., Space Technology Library, London, 2001, pp. 906–907.

[19] Gill, P. E., Murray, W., and Saunders, M. A., "SNOPT: An SQP Algorithm for Large-Scale Constrained Optimization," *SIAM Review*, Vol. 47, No. 1, 2005, pp. 99–131. doi:10.1137/S0036144504446096